Macromolecules
ARTICLE

Macromolecules **2010**, *43*, 9555–9566 **9555**
DOI: 10.1021/ma101897x

Dendritic versus Linear Polymer Brushes: Self-Consistent Field Modeling, Scaling Theory, and Experiments

Alexey A. Polotsky,[†] Torben Gillich,[‡] Oleg V. Borisov,*[,†,§] Frans A. M. Leermakers,[⊥] Marcus Textor,[‡] and Tatiana M. Birshtein[†]

[†]*Institute of Macromolecular Compounds of the Russian Academy of Sciences, St. Petersburg, Russia,* [‡]*Surface Science and Technology, ETH Zurich, Switzerland,* [§]*IPREM UMR 5254 CNRS/UPPA, Pau, France, and* [⊥]*Laboratory of Physical Chemistry and Colloid Science, Wageningen University, Wageningen, The Netherlands*

Received August 18, 2010; Revised Manuscript Received October 4, 2010

ABSTRACT: Equilibrium structural properties of polymer brushes formed by dendritic polymer chains (dendrons) are studied by means of Scheutjens−Fleer self-consistent field (SF-SCF) modeling and scaling analysis. Limiting cases of minimal and maximal possible losses of conformational entropy corresponding to different assumptions concerning distribution of elastic tension in the end-grafted dendrons are analyzed on the basis of the Flory-type scaling approach. The numerical SCF modeling indicates that the effective exponent of the power-law dependence for the height of dendritic brush on the grafting density differs from that derived within the Flory-type approximation. This is explained by changing of the intramolecular elastic tension distribution upon an increase in grafting density. The distributions of end and branching points are wide and exhibit multiple maxima, pointing to a broad distribution in the chain stretching. This distribution leads to monotonically decreasing overall density profiles. The theoretical results are in line with experimental findings on linear and dendritic poly(ethylene glycol) layers end-grafted onto TiO_2 surfaces.

1. Introduction

The polymer brush is among the best studied systems in polymer science. Brushes, formed by long polymer chains densely grafted to a solid−liquid or to a liquid−liquid interfaces, received ample attention from both theoretical and experimental perspectives.[1−3] Early works were motivated by the promise that brushes provide steric stabilization of colloidal dispersions. In such applications the repulsive forces that are found when two solvated brushes are forced to overlap can easily overcome the attractive van der Waals forces that would otherwise provoke aggregation and phase separation.[4,5] More recently, polymer brushes are being explored in tribological applications, i.e., for improving boundary lubrication. It was demonstrated that the friction coefficient between sliding surfaces decorated by a neutral or a charged polymer brushes is dramatically reduced as compared to that between bare surfaces.[6−10]

Further interest in polymer brushes is motivated by various applications in emerging domains such as biomaterial engineering and nanomedicine. Surfaces of artificial materials or biomedical devices may be modified by water-based multifunctional synthetic polymers. Upon contact with biofluids one may then anticipate a more favorable biological response. Surface immobilization of functionalized biocompatible polymers may result in antithrombogenic, antimicrobial, and/or anti-inflammatory responses, thus enhancing biocompatibility of biomaterials.[11] Brushes also occur in drug delivery systems. PEO grafts on lipid vesicles give stealthlike properties as these capsules remain unnoticed by the immune system. Moreover, these grafts may be used to carry ligands targeted to specific cells or tissues.[12,13] Brushes of biomacromolecules and synthetic macromolecules constitute the key structural motive in biochips for DNA/RNA, protein, and carbohydrate analysis, used in diagnostics and in the development of drugs.[14]

It has been well recognized that brushlike structures of biomacromolecules play an important role in living (biological) systems. For example, extracellular layers of branched polysaccharides decorate bacterial surface and mediate cell adhesion.[15] Aggrecan molecules (protein/polysaccharide molecular brushes) control mechanical stresses in synovial joints.[16] Neurofilaments (brushlike structures formed by nonstructured proteins) form the internal skeleton of neurons; they are responsible for the asymmetric elongated shape and are essential for the proper functioning of neurons.[17−21] Polymer brushes appear also as a key structural motive in self-assembled structures (micelles of all sorts and shapes) and mesophases formed by synthetic block copolymers and bioconjugates.[22]

First theoretical models focused on polymer brushes made of linear flexible polymer chains end-grafted onto a planar solid substrate and immersed into a good solvent. Both a Flory-type analysis and Alexander−de Gennes scaling approaches were elaborated.[23−26] It was proved that in a brush polymer chains are extended (strongly stretched) in the direction perpendicular to the grafting surface. When the grafting density is above a threshold, they do so proportionally to the contour length. This strong stretching is favorable as it reduces the crowding of the chains in the brush. The unfavorable free energy associated with the monomer−monomer contacts must be balanced by the corresponding conformational entropy loss due to stretching. An important result from such optimization is that the average polymer concentration in the planar brush is independent of the degree of polymerization of the grafted chains and fully controlled by the grafting density and solvent quality.

In recent years, the theory of polymer brushes has been extended and generalized in various directions. For example, in

*To whom correspondence should be addressed.

Published on Web 10/22/2010

many cases it proved relevant to take the curvature of the grafting surface into account.[27,28] The importance of the solvent quality for the brush structure has been discussed.[29] Polyelectrolyte brushes, which are brushes for which electrostatic interactions dominate, have been evaluated both for cases that the charges are quenched[30−32] or annealed (pH sensitive).[33] For dense brushes liquid-crystalline ordering is relevant, and both thermotropic and lyotropic interactions were accounted for.[34−36]

Deeper insights into the structural organization of polymer brushes have been obtained on the basis of the self-consistent field (SCF) theory[37−41] employing the strong chain stretching (quasi-classical) approximation.[42] It was demonstrated that individual chains in a brush exhibit strong fluctuations in their extension. This is exemplified by the result that the free ends of grafted chains are distributed throughout the brush layer. In combination with the nonuniform distribution of the local tension inside the chains, a broad distribution of the chain ends leads to a monotonic decay of the polymer concentration profile. These predictions of the analytical SCF theory were convincingly supported by computer simulations[43−49] and numerical Scheutjens−Fleer self-consistent field (SF-SCF) calculations.[50] The latter computational approach gives a more exact evaluation of the (mean field) partition function for chains in a brush, without some preassumption that the chains are strongly stretched. Hence, the SF-SCF method gives a more detailed description of the brush structure in a wide range of grafting densities.

To date, polymer brush theory almost exclusively focused on linear polymer chains. A few results for brushes composed of comblike and starlike macromolecules are reported in refs 51 and 52. In the meantime, however, advanced synthetic approaches now allow the making of macromolecules with a virtually arbitrary complex and well-controlled branched architecture (stars, combs, dendrons). Moreover, the technology to attach these to surfaces becomes available. It is believed that brushes from branched architectures may introduce novel desired features, such as enhanced stimuli responsiveness, outstanding nanomechanical properties, and tuned biointeractivity. More specifically, the large number of terminal segments (free ends) in grafted highly branched polymers offers an attractive opportunity to enlarge the number of (bio)functional groups that may be exposed to the solution. These may show an improved specific interactions (molecular recognition) with solute molecules. The latter property is of great importance in, e.g., diagnostic systems. In the colloidal domain, brushes formed by branched polymers may provide better steric stabilization of dispersions because of a higher polymer density in the protecting layer. Brushes composed of branched molecules may cause a sharper rise of the steric forces at small separations between the surfaces. From a physical point of view, brushes of branched macromolecules are challenging because the distribution of the elastic tension and the fluctuations of the individual molecules is far from trivial as these properties will differ from the behavior of the same molecules in solution.

Conformations of individual dendritic macromolecules in solutions have been extensively studied in past decades, both experimentally and theoretically (see e.g. ref 53 for a comprehensive review). The intramolecular structural organization of an individual dendritic (or "starburst") macromolecule remained a matter of debate for a long time. The first model proposed by de Gennes and Hervet[54] predicted a "hollow" dendrimer structure, wherein both the local polymer density and the degree of stretching of the spacers increased in the radial direction from the center to the periphery of the dendrimer. The hollow dendrimer model suggested to use dendrimers as molecular nanocontainers that may be loaded by active substances in drug-delivery applications. However, small-angle neutron and X-ray scattering unambiguously indicated a uniform distribution of polymer density in the intramolecular volume of dendritic macromolecules. These experimental results were supported by simulations[55] and numerical self-consistent field theory.[56,57] Meanwhile, scaling results for the size of dendrimers as a function of the architectural parameters were derived[56,57] and elaborated by computer simulation results.

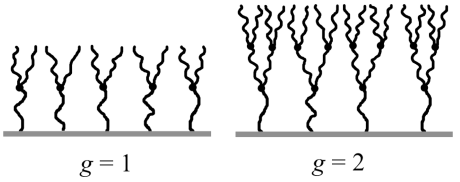

Figure 1. Schematic illustration for polymer dendron brush. In this example, the branching functionality $q = 2$, and $g = 1$ and 2 is the number of generations on the left and right, respectively.

The goal of the present paper is to reach a better understanding of the structural organization of dendritic polymer brushes. We use the self-consistent field theory and compare results to existing experiments. The paper is organized as follows. We start with discussing a theoretical model of a brush formed by dendrons grafted by the root terminal group to a planar substrate (section 2). In section 3 we present a simple Flory-like approach targeted to describe the structure of a dendritic brush. Here the focus is on limiting cases of minimal and maximal possible losses of conformational entropy that result from different assumptions with respect to the distribution of the elastic tension in end-grafted dendrons. In section 4 we briefly describe the principles of the Scheutjens−Fleer self-consistent field (SF-SCF) theory in the context of dendritic polymer brushes. In the results, section 5, we present a detailed comparative analysis of the structural organization of brushes formed by the second generation of dendrons and linear polymers. The effect of the number of generations is also analyzed in this section. In section 6 we describe the experimental system consisting of poly(ethylene glycol) (PEG) dendrons of the second generation, grafted to the TiO_2 surface through 3,4-dihydroxyphenylalanine (DOPA) terminal groups, summarize the experimental results obtained for the PEG dendritic brush, and compare these to results for brushes made by linear PEG molecules of approximately the same molecular weight. Finally, in section 7 we sum up our conclusions.

2. Theoretical Model of the Dendritic Polymer Brush

Let us focus on a brush formed by dendritic polymers (dendrons) grafted by the terminal (root) segment onto an impenetrable planar surface and immersed in a monomeric solvent. A schematic illustration is given in Figure 1. The grafting density, defined by the number of dendrons per unit surface area, is given by $1/s$ (s being the surface area per dendron).

We will assume that the distance, $\sqrt{s}$, between two neighboring dendrons is smaller than the characteristic size of the individual dendrons in a dilute solution. Hence, the dendrons strongly interact with each other, which is a prerequisite to be in the brush regime. In the opposite case, when the dendrons are far apart, the so-called mushroom regime is found. In such sparse grafting situation the conformations of each dendron are only weakly perturbed by the interactions with the surface, and we will not discuss this case further.

Let us further assume that the spacers in the grafted dendrons are intrinsically flexible. That is, the statistical segment length is on the order of monomer size a. Below we use a as the unit length. More specifically, our model mimics PEG dendrons with flexible poly(ethylene oxide) spacers which will be discussed in more detail in section 6.

Referring once again to Figure 1, each dendron is characterized by the generation g and a functionality $q = 2, 3, \ldots$ of each branching point. The functionality is defined as the ratio between

the number of spacers in generation $g + 1$ and that in generation g. The number of branching points in a dendron equals $(q^g - 1)/(q - 1)$. The number of monomer units per spacer is fixed throughout the molecule and is given by n. In passing, we mention that a generalization for the case of nonequal spacers lengths is straightforward. The number of monomer units in a dendron of generation $g = 0, 1, 2, ...$ equals

$$N = n(q^{g+1} - 1)/(q - 1) \approx nq^g \quad (1)$$

where the last approximation is reasonable for $g \gg 1$. It is easily checked that for $g = 0$ or $q = 1$, we return to a linear chain with length $N = n$ ("root spacer") or $N = n\,(g+1)$ segments, respectively.

We also introduce the number of monomer units in the longest path within the dendron. This path includes one spacer from each generation and comprises

$$\mathcal{N} = n(g+1) \quad (2)$$

monomer units. Obviously, for the linear chain ($g = 0$ or $q = 1$) $\mathcal{N} = N$. For dendrons, the ratio $N/\mathcal{N}$ does not depend on n and grows with an increase in both q and g. This ratio can be considered as a measure of the degree of branching in the dendron.

3. The Boxlike Model for a Dendritic Polymer Brush

We will first present results of a classical Flory-type anaylsis. This approach delivers power law (scaling) dependences of the characteristic thickness of the dendritic brush as a function of the grafting density $1/s$, the number of generations g, and the spacer length n. The Flory-type approach is known in the context of polymer brushes as the Alexander−de Gennes box model.[23,24] In this context one disregards gradients in the polymer density and basically ignores the distribution of the branching points and terminal segments in the direction perpendicular to the grafting surface. Similarly, as in most other approaches, the lateral (in-plane) homogeneity of the brush is preassumed as well.

The free energy per dendron (here and below all the free energies are expressed in k_BT units), which is part of a brush, can be split up in different contributions:

$$F(H) = F_{\mathrm{int}}(H) + F_{\mathrm{conf}}(H) \quad (3)$$

In this equation, H is the thickness (sometimes called height) of the brush. The height is the characteristic size of a dendron in the direction perpendicular to the surface. The first term in eq 3 describes the free energy contribution due to (repulsive) excluded-volume interactions in the brush. Under good solvent conditions, when it suffices to take binary contacts into account and neglect higher order terms, one may write

$$F_{\mathrm{int}} \cong vNc \quad (4)$$

In this equation, the mean-field estimate for the monomer−monomer contacts, Nc, is counted, where $c = NH^{-1}s^{-1}$ is the average concentration of the monomer units in the brush. Each encounter gives a free energy cost of v, which is the second (segment) virial coefficient (v is positive under good solvent conditions).

The second term in eq 3 contains the conformational entropy losses that are due to the extension of the polymer chains in the brush. The essential assumption of the boxlike model is that all chains in the brush are stretched fairly equally and uniformly in the direction perpendicular to the surface. In the case of a brush formed by linear chains, $g = 0$ or $q = 1$, this leads to the well-known Gaussian form for F_{conf}:

$$F_{\mathrm{conf}}^{(\mathrm{linear})} \cong \frac{H^2}{\mathcal{N}} \quad (5)$$

Note that this form for the conformational free energy loss allows for an unlimited extensibility of the chains (Gaussian chain model).

Balancing the entropic elasticity, eq 5, with the free energy of excluded-volume interactions, eq 4, leads to the expression for the height of a brush composed of linear chains:

$$H^{(\mathrm{linear})} \cong \mathcal{N}s^{-1/3} \quad (6)$$

and the average concentration of monomer units in the brush

$$c^{(\mathrm{linear})} \cong s^{-2/3} \quad (7)$$

The situation becomes more complex when the brush is formed by branched macromolecules. In this case, the use of the boxlike model implies certain *a priori* assumptions with respect to the distribution of the elastic tension within the branched macromolecules. Two possible limiting scenarios of the dendron stretching are distinguished. The first one corresponds to the stretching of the longest path only. This implies that a minimum number of spacers is stretched while the remaining ones remain unstretched. The second one corresponds to the stretching of all the spacers in the dendron. This leads to estimates for the minimal or maximal conformational entropy losses. In practice, we expect that the true stretching for molecules of a dendron brush is in between these limits and the true conformational entropy losses will be in between these two limiting values.

The first scenario assumes that only the (arbitrary) longest path in the dendron is stretched and all spacers that do not belong to this longest path are not deformed at all (remain Gaussian). This scenario corresponds to the smallest entropic penalty at given overall dimensions of the dendron. It is noticed that one has to satisfy, at each branching point, a balance of the entropic forces. Since the number of spacers in each generation increases as a function of the generation number, the average extension of the spacers in each generation decreases as a function of the number of the generation.[57] This is why we denote to the conformational entropy loss in this scenario with $F_{\mathrm{conf}}^{(\mathrm{nonuniform})}$. It is given by

$$F_{\mathrm{conf}}^{(\mathrm{nonuniform})}(H) \cong \frac{H^2}{\mathcal{N}} \quad (8)$$

which formally coincides with eq 5.

With increasing grafting density, the overall crowding increases, and therefore also the overall degree of stretching increases. That is why, depending on the degree of branching, it may become impossible that parts of the dendron remain undeformed/unstretched. In other words, upon increasing the grafting density, one may start to stretch also spacers that do not belong to the longest path.

In the second scenario it is assumed that all the spacers in all the generations are equally and uniformly stretched. A similar assumption, as with respect to the distribution of stretched spacers, has been proposed by Boris and Rubinstein for the conformational analysis of isolated dendrons in solution[56] and later was exploited by Kröger et al.[52] In this case the extension of each spacer is $\sim H/(g + 1)$, and the corresponding free energy cost is referred to as $F_{\mathrm{conf}}^{(\mathrm{uniform})}$. Since the total number of spacers equals N/n, we find

$$F_{\mathrm{conf}}^{(\mathrm{uniform})}(H) \cong \frac{NH^2}{n^2(g+1)^2} = \frac{H^2}{\mathcal{N}}\frac{N}{\mathcal{N}} \quad (9)$$

As compared to the first scenario, eq 8, the free energy given by eq 9 is larger by a factor $N/\mathcal{N} \gg 1$. Remarkably, similarly to the first

scenario, the second one corresponds to the limiting value of the free energy in scaling terms.

Minimization of the free energy given by eqs 3, 4, 8, and 9 leads to the following two limiting expressions for the equilibrium brush thickness

$$H \cong \begin{cases} N^{2/3}\mathcal{N}^{1/3}v^{1/3}s^{-1/3} = \mathcal{N}(N/\mathcal{N})^{2/3}v^{1/3}s^{-1/3}, & \text{longest path stretching} \\ N^{1/3}\mathcal{N}^{2/3}v^{1/3}s^{-1/3} = \mathcal{N}(N/\mathcal{N})^{1/3}v^{1/3}s^{-1/3}, & \text{uniform stretching} \end{cases} \tag{10}$$

and for the free energy

$$F \cong \begin{cases} N(N/\mathcal{N})^{1/3}v^{2/3}s^{-2/3}, & \text{longest path stretching} \\ N(N/\mathcal{N})^{2/3}v^{2/3}s^{-2/3}, & \text{uniform stretching} \end{cases} \tag{11}$$

which both reduce to the known expression for the brush formed by linear polymer chains when $N = \mathcal{N}$.

The corresponding average intrabrush polymer density is given by

$$c \cong \begin{cases} (N/\mathcal{N})^{1/3}v^{-1/3}s^{-2/3}, & \text{longest path stretching} \\ (N/\mathcal{N})^{2/3}v^{-1/3}s^{-2/3}, & \text{uniform stretching} \end{cases} \tag{12}$$

Comparing the two results for the boxlike model obtained for the two limiting assumptions for the elastic stretching of grafted dendrons, we find that the first one (only longest path stretching) leads to larger equilibrium heights, a lower intrabrush polymer density, and, correspondingly, a lower free energy. In order to avoid misunderstandings, let us mention again that in the first scenario the combination of a minimal free energy and a maximal stretching is connected with the extension of only a part of the dendron (namely, that of the longest path).

Hence, we find that, irrespectively of the assumption concerning the distribution of stretching in the dendrons, in the box model the limiting values for the brush thickness scale as $s^{-1/3}$. Moreover, the average polymer density in the brush and the free energy per molecule scale as $s^{-2/3}$. Both results are also known for brushes formed by linear polymers.

In contrast to brushes formed by linear chains, the structural properties of the dendritic brush depend not only on the number of monomers in a dendron N but also on the degree of branching, $N/\mathcal{N} \geq 1$. The exponent of the power law dependence of the dendritic brush thickness on the degree of branching $N/\mathcal{N}$ is essentially affected by the "stretching scenario" of the dendrons in the brush and is different for the two limiting cases.

Let us introduce the concept of the "equivalent brush", that is, a brush formed by linear chains with chain length, $N^{(\text{linear})}$, and grafting density, $1/s^{(\text{linear})}$, chosen such that the brush thickness and the average polymer concentration in the equivalent linear brush, as calculated according to the eqs 6 and 7, coincide with the limiting expressions for the dendritic brush given by eqs 10 and 12.

The parameters of the equivalent brushes that correspond to the two stretching scenarios are

$$N^{(\text{linear})} \cong \begin{cases} \mathcal{N}(N/\mathcal{N})^{1/2}, & \text{longest path stretching} \\ \mathcal{N}, & \text{uniform stretching} \end{cases} \tag{13}$$

and

$$s^{(\text{linear})} \cong \begin{cases} s(N/\mathcal{N})^{-1/2}, & \text{longest path stretching} \\ s(N/\mathcal{N})^{-1}, & \text{uniform stretching} \end{cases} \tag{14}$$

As one can see from eqs 13 and 14, in both equivalent brushes the number of monomer units per unit area $N^{(\text{linear})}/s^{(\text{linear})} = N/s$ coincides with that in the dendritic brush.

The brush composed of linear chains that is equivalent to the dendritic brush in the limit of its minimal density and maximal height is composed of linear chains whose length is the geometric mean of N and $\mathcal{N}$. The corresponding grafting density is $(N/\mathcal{N})^{1/2}$ higher than in the dendritic brush.

The brush composed of linear chains, which is equivalent to the dendritic brush in the limit of its maximal density and minimal height, is composed of linear chains with the same length as the length of the longest path in the dendron, $\mathcal{N}$, and grafted to the surface with a density that is $N/\mathcal{N}$ times larger than the grafting density in the dendritic brush.

When experimental results are analyzed, the structural properties of the dendritic brush are often compared to those of the brush formed by linear polymers of the same degree of polymerization, N, grafted with the same surface area per molecule, s. As it follows from eqs 10 and 12, the ratio of the height of the dendritic brush to the height of the brush made of linear chains is smaller than unity and should be found in the limits

$$\frac{H^{(\text{dendron})}(N,s)}{H^{(\text{linear})}(N,s)} \cong \begin{cases} (N/\mathcal{N})^{-1/3}, & \text{longest path stretching} \\ (N/\mathcal{N})^{-2/3}, & \text{uniform stretching} \end{cases} \tag{15}$$

Correspondingly, the polymer density in the dendritic brush is larger than that in the brush formed by linear chains and the ratio of the two values should be found in the range

$$\frac{c^{(\text{dendron})}(N,s)}{c^{(\text{linear})}(N,s)} \cong \begin{cases} (N/\mathcal{N})^{1/3}, & \text{longest path stretching} \\ (N/\mathcal{N})^{2/3}, & \text{uniform stretching} \end{cases} \tag{16}$$

Results obtained thus far demonstrate the limited power of the boxlike model for brushes formed by branched polymers. Scaling estimates allow us to identify only the boundaries of the (possible) mean characteristics of the dendritic brush. For a more detailed description of the brush structure it is necessary to turn to the more detailed SCF method. In the following paragraph we will outline an approach that needs no *a priori* assumptions about the tension distribution in dendrons. All monomer interactions (not only the binary) and the finite extensibility of the spacers are properly taken into account.

4. SCF Formalism

The self-consistent field method is well-known for the modeling of inhomogeneous polymer layers.[5,58] At the basis of the approach is a mean-field free energy which features segment volume fraction profiles (for both polymer segments and solvent molecules) as well as corresponding segment potentials. The evaluation of this free energy requires a chain model (we will use the freely jointed chain model) and needs information on how the polymer solvent interactions are accounted for. Classically, nearest-neighbor interactions parametrized by Flory−Huggins interaction parameters are used for this. Below we will focus exclusively on good solvent conditions, for which $\chi = 0$. We follow Scheutjens and Fleer, who suggested to use a lattice with characteristic lattice site size a equal to the segment size. These authors also opted for a local incompressibility relation, which in words says that the polymer volume fraction plus that of the solvent add up to unity (no free volume). The optimization of the free energy resulted in two additional so-called SCF requirements. One requirements leads to the protocol of how the volume fractions are computed from the potentials, and the other one specifies how the potentials are found from the volume fractions.

The SF-SCF method solves these mutually entangled SCF equations numerically, so that the mean-field free energy for (in this case) a brush of dendritic molecules can be evaluated.

Without going into all details, a few additional pieces of information may be useful.

For the macromolecular species it is necessary to know the statistical weights of all possible and allowed conformations. These weights are collected in the single chain partition function Q. The SF-SCF method closely follows the Edwards diffusion equation approach which leads to Q in a very efficient manner once the self-consistent potential field u, created by all the molecules in the brush, is available. We may introduce the distribution function $G(z',z;n)$ as the statistical weight of a chain fragment with a length n having its ends fixed in the points z' and z. According to Edwards, this distribution functions obey the diffusion equation

$$\frac{\partial G(z',z;n)}{\partial n} = \frac{a^2}{6}\frac{\partial^2 G(z',z;n)}{\partial z^2} - \frac{u(z)}{k_B T}G(z',z;n) \qquad (17)$$

Here we implement the one-gradient version of the SF-SCF method which assumes that the brush is laterally uniform: all the local properties (that is, the polymer densities φ (equivalent to the dimensionless concentration c) and, conjugated to these, the self-consistent potentials, u) vary only in the direction perpendicular to the grafting surface. This means that these depend on the z coordinate, but not on the lateral coordinates (x, y). The presence of an impenetrable solid surface specifies the boundary condition at $z = 0$. The system size in the z-direction is chosen large enough so that the polymer density vanished and reflecting boundary conditions suffice. The grafting of the chain end (root spacer) onto the solid−liquid interface is taken care of by the initial conditions. Whereas the application of eq 17 implies the use of Gaussian chain statistics, the mapping of this equation onto a lattice implies a change of the chain model into the freely jointed chain (FJC). This change is relevant only in the limit of stretching up to the contour length. Unlike the Gaussian chain, the FJC has a finite extensibility. In this chain model, the chains are fully flexible, and one can imagine the method as a step-weighted random walk that follows the chain architecture and implement this on a lattice. The lattice constants determine *a priori* probabilities of steps in different directions, which are further multiplied by the Boltzmann factors dependent on the spacial distribution of the self-consistent potential field. Many details of the SF-SCF method are readily available in the literature.[5] For the details of the SF-SCF calculations in the particular case of polymers with some branched topology see, for example, ref 57.

The calculations were performed using the SFBox program developed at Wageningen University. From these calculations we get access to a wide range of conformational properties of the macromolecules in the brush. The program outputs the local structural properties (distributions of all the segments including terminal and branching points) as well as integral properties (the average thickness of the brush) without any preassumptions concerning of the dendrons in the brush. In addition, using SFBox, one can analyze how the elastic tension is distributed over the spacers of different generations within individual dendrons. It thus allows us to identify which of the limiting scenarios that were described in the scaling analysis correspond to the equilibrium state.

5. Dendritic versus Linear Polymer Brushes: SCF Results

5.1. Brushes Formed by Dendrons of the First Generation. In this subsection we collect results of the SF-SCF method and analyze the structural properties of brushes formed by dendrons of the first generation, $g = 1$.

We start with an analysis of the structure of brushes formed by dendrons with functionality $q = 3$ and compare these systematically to that of brushes formed by linear polymer chains. For this particular choice of parameters the total degree of polymerization of the dendron $N^{(\mathrm{dendron})} = (1 + q)n = 4n$; the longest path is $\mathcal{N}^{(\mathrm{dendron})} = (1 + g)n = 2n$ and $N^{(\mathrm{dendron})}/\mathcal{N}^{(\mathrm{dendron})} = 2$.

According to the predictions of the box model (cf. section 3, eqs 13 and 14), two equivalent brushes, composed of linear chains, give scaling limits for the possible values of the main brush characteristics—the brush thickness H and the average polymer density within the brush c. We will compare results of the SF-SCF approach for dendritic brush with these two equivalent linear chain brushes. Since these equivalent brushes determine the values of the minimal and the maximal possible free energy (and polymer density as well) of the dendritic brush, we will refer to these as the lower and upper boundaries, respectively. In accordance with eqs 13 and 14, linear brushes with the following characteristics will be considered.

Lower boundary. Linear chains with a degree of polymerization $N^{(\mathrm{linear})} = (2\sqrt{2})n$ with grafting density $s^{(\mathrm{linear})} = s^{(\mathrm{dendron})}/\sqrt{2}$.

Upper boundary. Linear chains with a length given by the longest path, $\mathrm{N}^{(\mathrm{linear})} = \mathrm{N}^{(\mathrm{dendron})} = 2n$, and doubled grafting density, $s^{(\mathrm{linear})} = s^{(\mathrm{dendron})}/2$.

For ease of comparison to the experiments, we consider also brushes formed by linear chains with the same total molecular weight $N^{(\mathrm{linear})} = N^{(\mathrm{dendron})} = 4n$ (that is, doubled number of monomer units in the longest path, $\mathcal{N}^{(\mathrm{linear})} = 2\mathcal{N}^{(\mathrm{dendron})} = 4n$) and the same grafting density, $s^{(\mathrm{linear})} = s^{(\mathrm{dendron})}$. Unless mentioned otherwise, we have used a spacer length of $n = 100$ segments.

5.1.1. Overall Polymer Volume Fraction Profile. In Figure 2, the overall density profiles for the dendritic brush ($g = 1$ and $q = 3$) and for the two equivalent linear chain brushes are plotted for various grafting densities. In panel (a) the density is given as a function of the distance, whereas in panel (b) the density is given as a function of the squared distance from the grafting surface. The latter coordinates are motivated by the fact that a parabolic volume fraction profile is linearized. For brushes composed of sufficiently long linear chains the parabolic profile is well established.[37−40] Not unexpectedly, in the brushes formed by linear chains, the polymer concentration profiles follows this parabolic shape for moderate grafting densities ($c(z^2)$ are reasonably linear). The depletion region very near the surface, best seen in Figure 2a, is caused by local conformational restrictions imposed by the impenetrable surface. All profiles show a smooth (exponential) decay of the polymer density at the edge of the brush. These are due to Gaussian fluctuation of nonstretched terminal segments of the chains. Deviations of the density profiles from the parabolic shape become progressively more and more important when the grafting density (also for linear chains) is increased. These deviations are known to arise from higher order repulsive interactions in the brush (third virial coeffient).[39,40] Moreover, for high grafting densities, effects of the finite extensibility of the chains (non-Gaussian elasticity) come into play.[44−49]

The shape of the density profile in the dendritic brush is, qualitatively, similar to that in the linear brush. From Figure 2a we find that, at moderate grafting densities, the polymer density profile in the dendritic brush follows almost exactly the density profile in the equivalent brush with $N^{(\mathrm{linear})} = 2\sqrt{2}n$ and grafting density $s^{(\mathrm{linear})} = s^{(\mathrm{dendron})}/\sqrt{2}$ (corresponding to the longest path stretching limit). This indicates that in this range of the grafting densities the elastic tension propagates predominately through the longest path of the end-grafted dendron, whereas the side paths are not stretched. Clearly, the equivalent linear brush with $\mathcal{N}^{(\mathrm{linear})} = \mathcal{N}^{(\mathrm{dendron})} = 2n$ and doubled grafting density, $s^{(\mathrm{linear})} = s^{(\mathrm{dendron})}/2$, which mimics the dendritic brush under the uniform stretching scenario, is more compact that the dendritic brush. However, upon the increase in grafting density, the dendritic brush becomes more compact than the equivalent

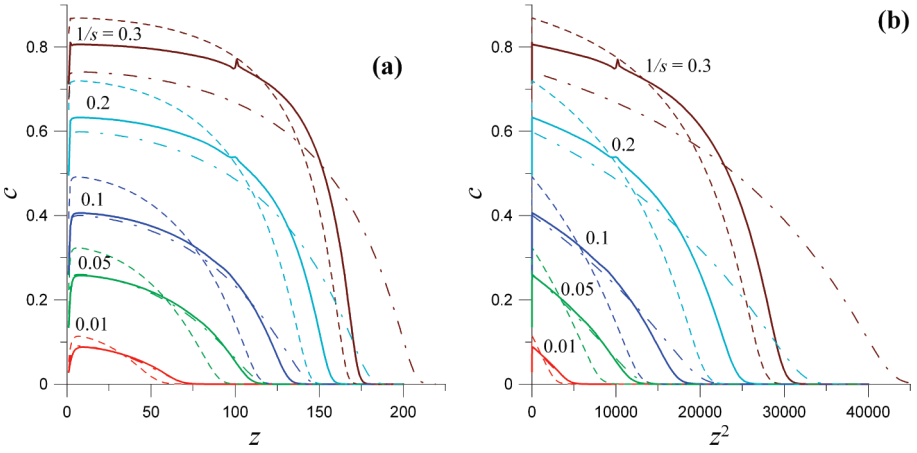

Figure 2. Polymer density profiles for the first generation dendritic brush with $g = 1$, $q = 3$ (solid lines) and for the two equivalent brushes (corresponding to the limits of uniform stretching, dashed lines, and to the longest path stretching, dash-dotted lines) plotted for various grafting densities $1/s$ as indicated, as a function of (a) the distance z and (b) the squared distance z^2 from the grafting surface.

brush that corresponds to the longest path stretching limit. At high grafting densities, the polymer density in the central region of the dendritic brush is larger than that in the equivalent brush that corresponds to the longest path stretching limit but smaller than that in the equivalent brush that corresponds to the uniform stretching limit. This implies that, upon an increase in the grafting density, not only the longest but also the side paths in the dendrons progressively become more and more stretched.

In Figure 2b, the polymer profiles for dendritic brushes are plotted as a function of square distance from the grafting surface. At relatively low grafting densities, where binary monomer−monomer interactions dominate over higher order ones and where the spacers obey Gaussian elasticity, the profiles clearly exhibit two distinguishable ranges, both with a quadratic decay of the volume fraction. The absolute value of the slope is smaller in the region proximal to the grafting surface and larger in the peripheral region of the brush. The existence of these two characteristic ranges in the polymer density profile suggests a stratified internal structural organization in the brush. This feature will be discussed in more details below. At higher grafting densities, similarly to what is observed for linear polymer brushes, the polymer concentration profile in the dendritic brush still exhibits a monotonic decay. The profile, however, cannot be fitted by a quadratic dependence; that is, the profile is not parabolic. Comparison of the density profile of a dendritic brush with that formed by linear chains of the same degrees of polymerization, $N^{(\mathrm{linear})} = N^{(\mathrm{dendron})}$, and grafting density, $s^{(\mathrm{linear})} = s^{(\mathrm{dendron})}$, indicates that in the dendritic brush the average density is larger and the characteristic brush height is smaller than that in the linear chain brush.

Let us next decompose the overall density profile into contributions from different fragments of grafted polymers. In Figure 3, we present the density distributions for the monomer units that belong (a) to the root and (b) to the terminal spacers of the dendrons. For comparison, in panel (c) we present, for a brush composed of linear chains, the volume fractions that come from the chain fragment bracketed by the grafting point (at the surface) and the middle of the chain and in (d) the remainder, that is, the volume fractions that are generated by the fragment from the middle of the chain to the free end. Comparison of panels (a) and (b), with panels (c) and (d), indicates that, in contrast to linear brushes (c, d), the proximal to the surface and central regions of the dendritic brush are significantly enriched by the monomer units that belong to the last generation spacers of the dendrons. This may indicate that either there is a large probability of turning back to the surface for the terminal spacers or, alternatively, there exists a large population of dendrons with a weakly extended root spacer.

The former option is extensively discussed in the literature as an option to fill the interior of dendritic molecules by segments of outer generations, which leads to a uniform packing of segments within the dendron. However, as we will demonstrate below, the second option (nonequal stretching) corresponds to the equilibrium structure of dendritic brushes.

Distributions shown in Figures 3a,b have a specific feature at high grafting density $1/s = 0.3$: there is a break in the root spacers density profile (Figure 3a) at $z = 100$, corresponding to the maximum possible extension of the root spacer which is accompanied by the jumpwise increase in the density of terminal spacer (Figure 3b).

An experimentally accessible structural property of the brush is its average thickness or, equivalently, the average concentration of the monomer units, as a function of the grafting density. The predictions of scaling theory[23−26] for brushes formed by linear chains, $H^{(\mathrm{linear})} \sim s^{-1/3}$ and $c^{(\mathrm{linear})} \sim s^{-2/3}$, were confirmed by a multitude of experimental works and by computer simulations. As specified by eqs 10 and 12, the boxlike model predicts the same scaling dependences for the thickness and monomer density in dendritic polymer brushes as a function of the grafting density under both limiting scenarios of the dendron stretching.

In Figure 4, the average concentration of the monomer units $\langle c\rangle = \sum_z c^2(z)/\sum_z c(z)$ in the brush is plotted as a function of the grafting density, $1/s$, in double-logarithmic coordinates. Here we used dendron brushes formed by the first-generation dendrons with progressively increasing functionality of the branching point $q = 2, 3, 4$) in panels a, b, and c, respectively. The two parallel straight lines in each panel correspond to the two limiting scenario of the dendrons stretching, which both have a slope 2/3, but are shifted with respect to each other by the value $^1/_3[\ln (1 + q)/2]$ according to eqs 12, 1, and 2.

As follows from Figure 4, at moderate grafting densities, the average concentrations of monomer units in dendritic brushes follow the scaling prediction $\langle c\rangle \sim s^{-2/3}$ accurately. However, upon an increase in the grafting density, the slope of $\log\langle c\rangle$ versus $\log(1/s)$ progressively increases. Clearly with increasing density, the concentration $\langle c\rangle(1/s)$ gradually departs from the lower toward the upper reference line. This increase in the slope of the $\log\langle c\rangle$ vs $\log(1/s)$ curves can be

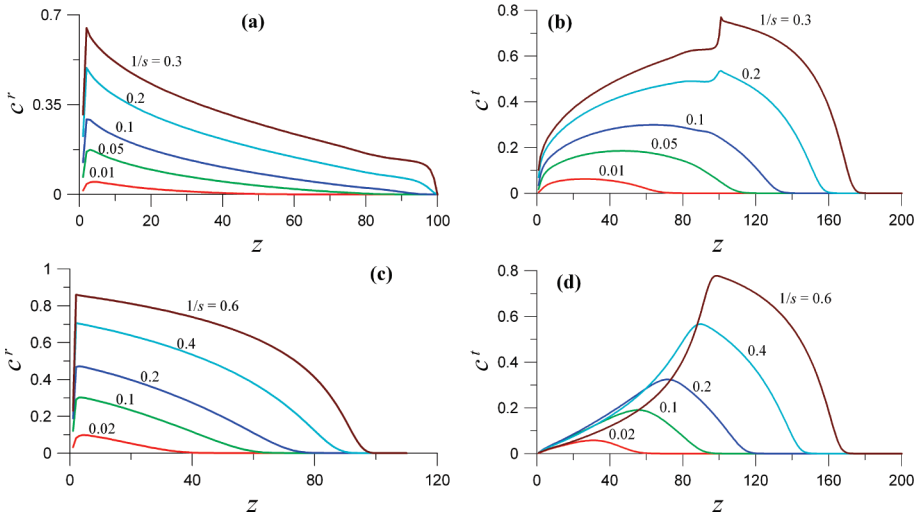

Figure 3. Concentration profile $c^r(z)$ of (a) the monomer units belonging to the root and (b) $c^t(z)$ for segments that belong to the terminal spacers of the first generation dendrons ($g = 1, q = 3$). Volume fraction profiles for a linear brush: (c) the first half of segments $c^r \equiv c(z, k = 1, ..., N/2)$, where $k = 1$ is the grafting segment, and (d) the second half of segments $c^t \equiv c(z, k = N/2, ..., N)$.

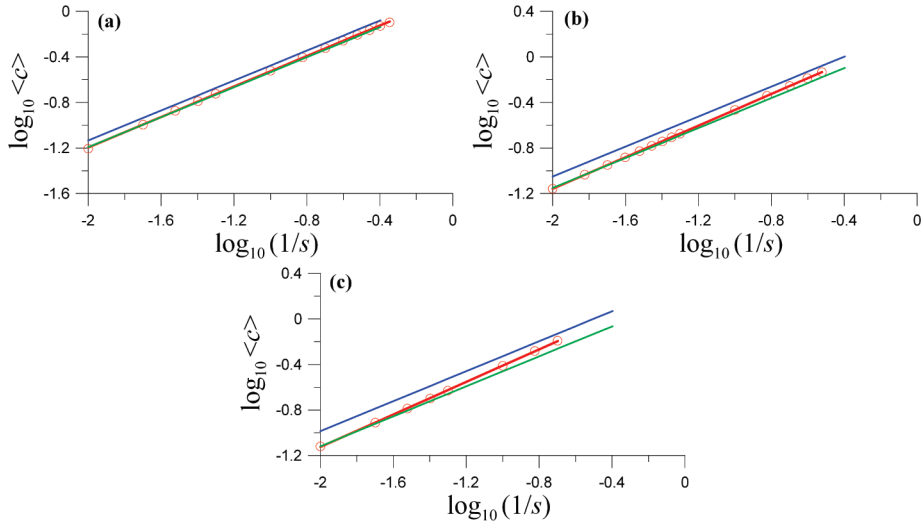

Figure 4. Dependences of the average concentration of the monomer units in a first-generation dendritic brush, $\langle c \rangle$, on the grafting density, $1/s$ (in double-logarithmic coordinates), for brushes with functionality of the branching point (a) $q = 2$, (b) $q = 3$, and (c) $q = 4$. The two parallel straight lines in each panel correspond to the two stretching limits, namely the stretching of the longest path only (lower line) and the uniform stretching (upper line). Both lines have a slope 2/3 and are shifted with respect to each other by the value $^1/_3[\ln (1 + q)/2]$.

ascribed to a progressive involvement of multiple "side" branches of the dendron in the stretching. This means that there is a gradual evolution from the stretching of the longest path only toward more uniform distribution of stretching among the branches of the dendron, as described above. The latter scenario plays an important role at high grafting densities (strongly crowded dendrons), whereas the former scenario occurs at moderately dense grafting.

The larger is the functionality of the branching points, the more pronounced is the transition between two stretching regimes. This is accompanied by a larger apparent exponent of the $\langle c \rangle$ vs $(1/s)$ dependences. The shift is better seen in Figure 4c than in 4a. It is worth mentioning that at large grafting densities and for large q the concentration of the monomer units in the brush is so large that higher order excluded-volume contributions (e.g., ternary) may become important. Moreover, the extensions of the spacers in the dendrons may approach their contour length. As a result, finite extensibility effects may come into play. In other words, the spacers do not obey Gaussian elasticity. Both reasons may also lead to a stronger increase of the polymer density as a function of the grafting density as predicted by scaling theory.

5.1.2. End and Branching Points Distributions. Figure 5a,b presents how the distributions of the terminal segments (that is, free ends) and that of the branching points, respectively, evolve for a dendritic brush upon an increase in the grafting density. For comparison, in Figure 6a,b the distributions of the free ends and the middle segments are presented for the reference polymer brush formed by linear chains. In both figures we have multiplied the volume fraction distribution by the area per molecule so that the integrals under the curves are the same. For the brush formed by linear chains, both distributions are unimodal and retain approximately the same shape. With increasing grafting density (decreasing s) there is a systematic shift of the most likely position of the end points (Figure 6a) as well as the middle points (Figure 6b) toward larger z values. These trends are well documented and follow the predictions of the analytical SCF theory.[37,39,40] In stark contrast, for dendritic brushes both the free end and the branching point distributions

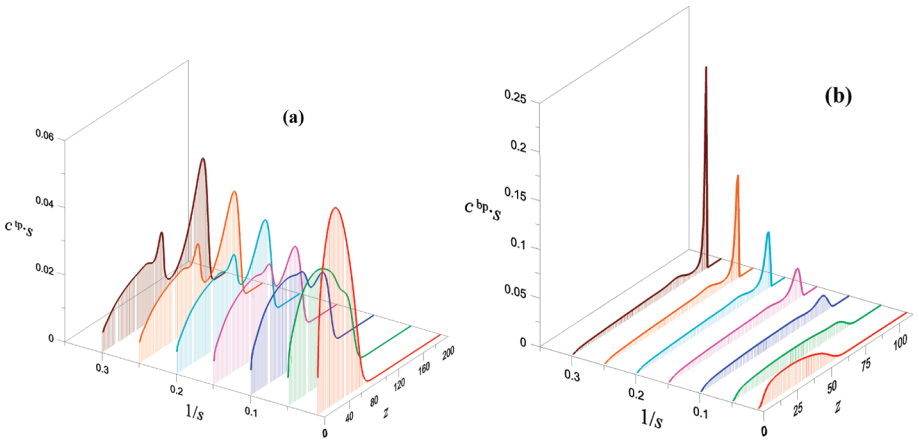

Figure 5. (a) Number distribution of the free ends (terminal segments), $sc^{tp}(z)$. (b) Number distribution of the branching points, $sc^{bp}(z)$, for a first-generation dendritic brush with $g = 1$ and $q = 3$ for different grafting densities $1/s$ as indicated.

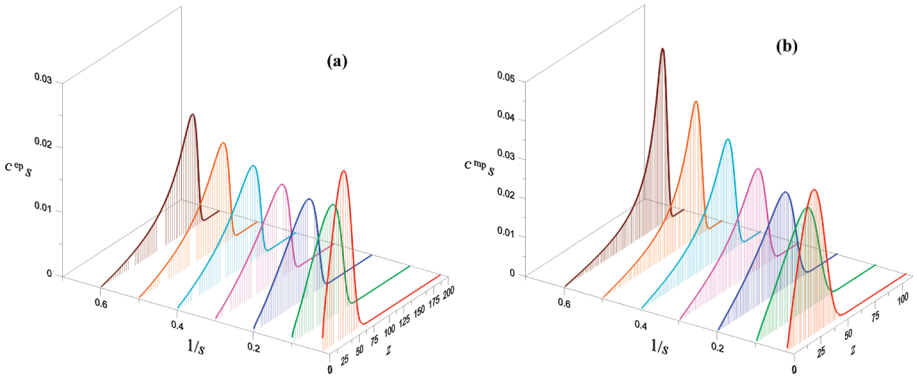

Figure 6. (a) Number distribution of free ends $sc^{ep}(z)$ and (b) number distribution of monomer units exactly halfway the chain (middle segments), $sc^{mp} = s\varphi(z, N/2)$, for the equivalent brush (that is as compared to the brush presented in Figure 5) composed of linear polymer chains.

exhibit two modes. First, there is a wide (plateau-like) proximal maximum found in the range between the surface and the edge of the brush for the terminal point (Figure 5a) or in the range from the surface to approximately halfway the brush height for the branching points (Figure 5b). Second, there is a more sharp maximum, which at small grafting densities (large $1/s$) appears as a shoulder, found at the edge of the brush for the terminal points (Figure 5a) or found in the middle of the brush for the branching points (Figure 5b). The latter maximum is located exactly at the maximal stretching position for the end of the root spacer ($z \approx 100$) and becomes significantly sharper at higher grafting densities. These bimodal distributions suggest that the set of conformations realized by dendrons in a dense brush is splitted into two distinct subpopulations.

The existence of two populations of dendrons—one which has a strongly, almost completely, extended root spacer and another one with a weakly extended root spacer—is illustrated in Figure 7. The subpopulation with less stretched root spacers contributes to the wide maximum in the distribution of the branching points proximal to the grafting surface as seen in Figure 5a. The existence of two populations of dendron conformations is manifested in two stratified regions of quadratic decay in the overall polymer density profile as noticed at modest grafting densities in Figure 2b. Such a stratified layer is known to exist in brushes composed of two linear chains that differ in length, the so-called bidisperse brush.[59] These findings clearly indicate that the filling of space in a densely grafted dendritic brush is not achieved by back-folding of the terminal spacers, but rather by the splitting of the dendrons in two populations with

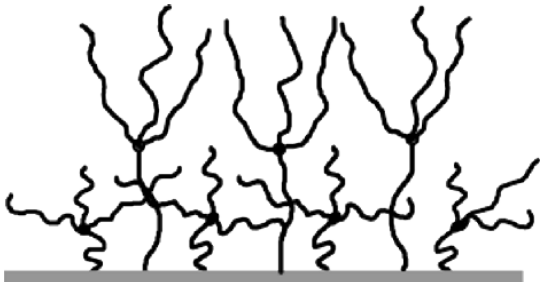

Figure 7. Schematic illustration of the occurrence of two populations of conformations of dendrons in a $g = 1$ dendritic brush.

strongly and weakly extended root spacers. The strongly stretched subpopulation of dendrons fills the periphery of the brush, whereas the weakly stretched or virtually unstretched subpopulation fills the interior of the brush.

5.2. Effect of the Number of Generations. An increase in the number of generations, g, in the dendrons leads similarly to an increase in the branching points functionality, q, to an increase in the branching parameter $N/\mathcal{N}$. For different generations, namely $g = 2$ and $g = 3$, we present the polymer density profiles $c(z)$ as well as $c(z^2)$ in Figure 8. The corresponding distributions of the end segments and of the branching points are presented in Figure 9. The most relevant points of these complex profiles will be discussed.

Upon an increase in the number of generations, the overall polymer density profiles flattens in the central part of the brush. The polymer density plotted as a function of square

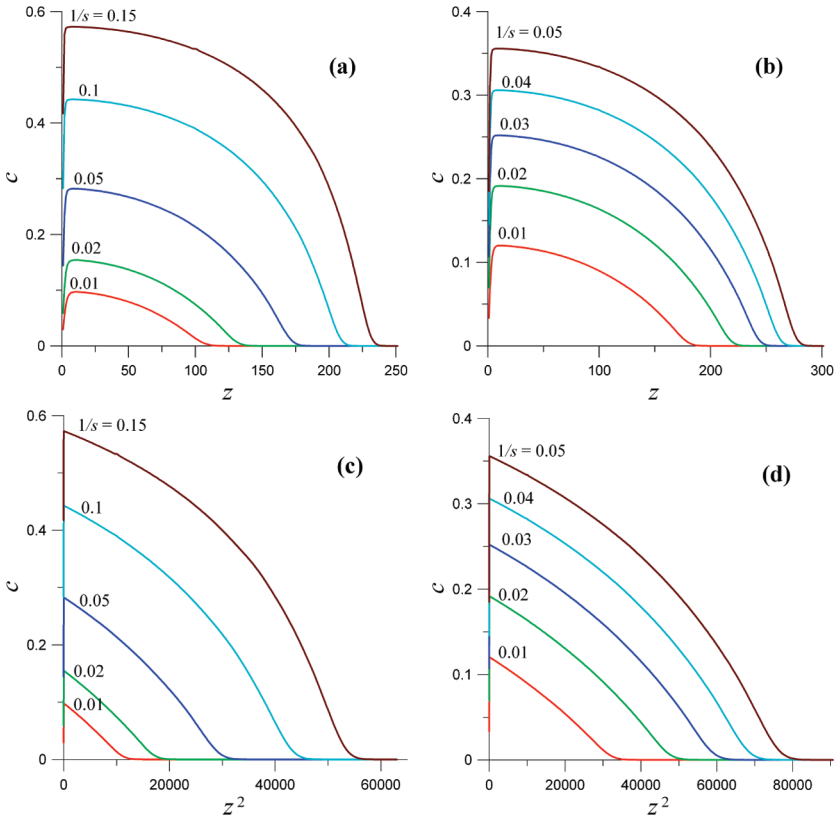

Figure 8. Polymer density profiles $c(z)$ or $c(z^2)$ for the brushes formed by dendrons of (a, c) the second generation $g = 2$ and (b, d) the third generation $g = 3$. In panels a and b the profiles are plotted as a function of z and in panels c and d as a function of z^2. In all cases $q = 2$.

distance from the surface exhibit, again at moderate grafting densities, several quasi-linear regions with progressively increasing slopes. Following the arguments given above, this points to a stratified internal organization of these brushes and to a multimodal distribution in the extension of the spacers of each particular generation. This stratified organization is confirmed by the complex patterns with multiple maxima found in the corresponding end and branching points distributions. The multimodal character of the distributions is most pronounced at intermediate grafting densities. Upon an increase in the grafting density the distributions of the end points of spacers of inner generations get stronly peaked. In particular, a sharp peak in the distribution of the end segments of the root spacers appears at $z \leq 100$; i.e., the root spacers approach the limit of the extensibility. Remarkably, even at high grafting density the terminal segments, as well as branching points of higher generations, are distributed throughout the brush.

In Figure 10, the average polymer concentration in the dendritic brush of generations $g = 2, 3, 4$ ($q = 2$) is plotted as a function of the grafting density $1/s$ in double-logarithmic coordinates. As in Figure 4 two parallel reference lines, corresponding to the two limiting stretching scenarios, are also plotted. Consistent with the brush formed by the first-generation dendrons (Figure 4), we find that the slopes of the $\log\langle c\rangle$ vs $\log(1/s)$ curves are close to 2/3, as predicted by the boxlike model, for both moderate and high grafting densities. In the intermediate range of grafting densities, the effective power law exponent is larger than 2/3. The deviation from the 2/3 power law appears at lower grafting densities and is more pronounced for dendrons of higher generations. The deviations, thus, are more pronounced for systems with larger values of the branching parameter $N/\mathcal{N}$. This feature is analogous to that observed for dendron brushes of the first generation upon an increase in the functionality q of the branching points. Hence, we can conclude that for dendrons with a higher number of generations the shift from the longest path stretching toward the uniform stretching regime, that is, the progressive increase of the stretching of the side paths, occurs already at lower grafting densities.

6. Experimental Results and Comparison to the Theory

Poly(ethylene glycol) (PEG) dendrons were bound to a titanium oxide (TiO_2) surface through a variable number of anchor groups of 3,4-dihydroxyphenylalanine (DOPA) moieties. In particular, the dendrons with 2, 3, and 4 DOPA groups in the anchor moiety (denoted as G2-DOPA$_2$, G2-DOPA$_3$, and G2-DOPA$_4$, respectively) were investigated. In addition, brushes formed by linear PEG chains (PEG-2300-DOPA$_4$, M = 3229 Da, DP_{PEG} = 56) were studied. These chains had approximately the same molecular weight as the PEG dendron and had four DOPA molecules as the anchoring moiety. All the dendrons, as well as the linear analogue, were adsorbed on TiO_2 surfaces via a dip and rinse method. The presence of a variable number of DOPA molecules in the anchor group provides different strengths of binding of the dendrons to the surface. In this way it is possible to vary systematically the grafting density.

The properties of the resulting polymer brushes were investigated using ex-situ ellipsometry and an in-situ quartz crystal microbalance with dissipation (QCM-D). With ellipsometry one can measure for a dry sample the polymer mass adsorbed on the TiO_2, and this gives the number of dendrons adsorbed per unit area of the surface. The QCM-D technique is used to measure the mass of the hydrated polymer brush, including solvent molecules, that are coupled to the polymer layer (hydration water). By comparing the results obtained by ellipsometry and QCM-D, the hydration of the polymer layer (in weight %) and the thickness of the hydrated polymer brush were calculated.

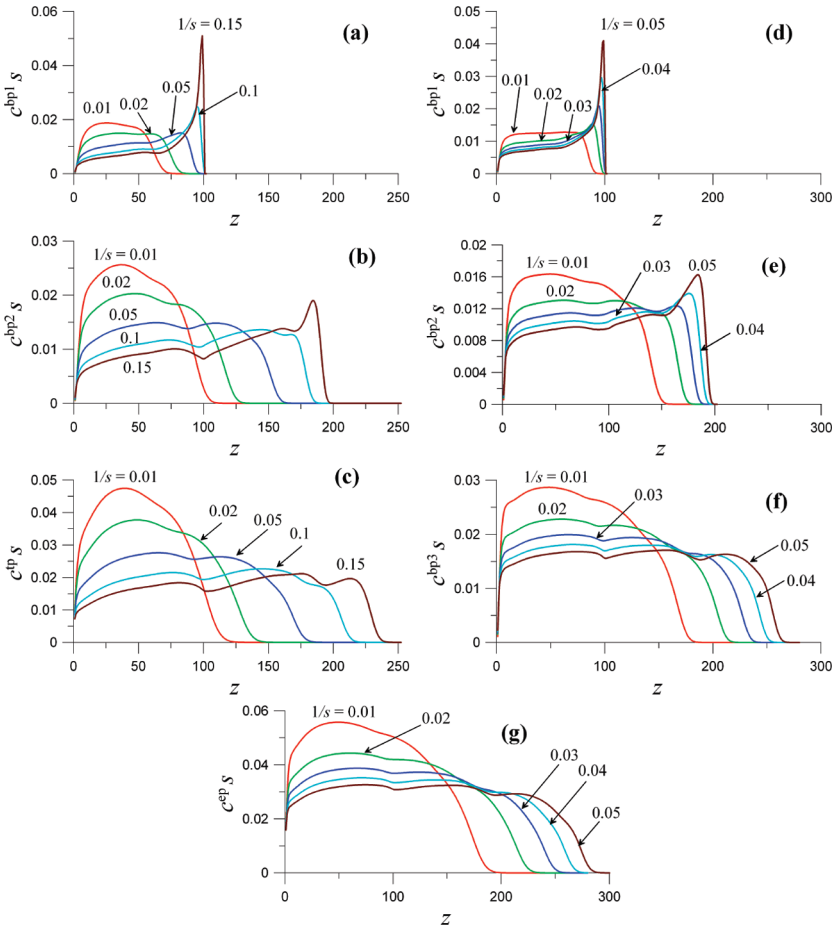

Figure 9. Number distributions of specified segments in dentron brushes of generation $g = 2$ and $g = 3$ for various values of the grafting density $1/s$ as indicated: (a) the distribution of the branch point between spacers of generation 0 and 1 in $g = 2$: $sc^{bp1}(z)$; (b) the distribution of the branch point between spacers of generation 1 and 2 in $g = 2$: $sc^{bp2}(z)$; (c) the distributions of the end segments in $g = 2c^{tp}(z)$; (d) the distribution of the branch point between spacers of generation 0 and 1 in $g = 3$: $sc^{bp1}(z)$; (e) the distribution of the branch point between spacers of generation 1 and 2 in $g = 3$: $sc^{bp2}(z)$; (f) the distribution of the branch point between spacers of generation 2 and 3 in $g = 3$: $sc^{bp3}(z)$; and (g) the distributions of the end segments in $g = 3c^{ep}(z)$.

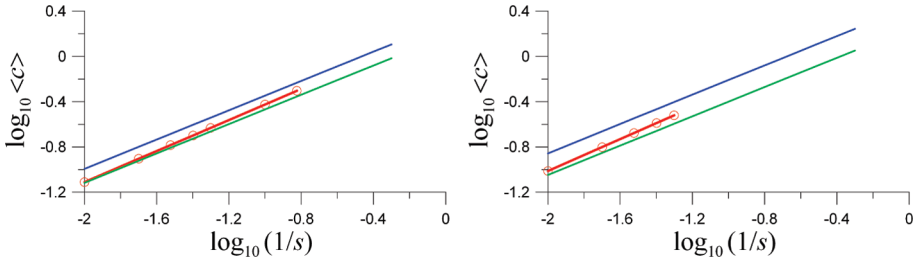

Figure 10. Average polymer concentration $\langle c \rangle$ in the dendritic brush of generations $g = 2, 3$ ($q = 2$) as a function of the grafting density $1/s$ (in double-logarithmic coordinates). The lower and the upper reference lines with the slopes 2/3 correspond to the limits of the longest path and uniform stretching, respectively.

Table 1. Parameters of the Dendritic (G2-DOPA$_4$, M_w = 2969.29 g/mol) and Linear Chain (PEG-2300-DOPA$_4$, M_w = 3229.70 g/mol) Brushes Obtained after 4.5 h of Adsorption

molecule	dry mass (ng/cm^2)	hydrated mass (ng/cm^2)	hydration (fraction)
G2-DOPA$_4$	196 ± 5	340 ± 15	42
PEG-2300-DOPA$_4$	165 ± 3	686 ± 16	76

The results obtained by ellipsometry and by QCM-D after 4.5 h of adsorption are summarized in Table 1.

The dry mass of the adsorbed PEG layer (per cm^2) was calculated from the ellipsometry data by

$$m^{(\text{ellipsometry})} = dl \quad [\text{g/cm}^2] \tag{18}$$

where $d = 1.05$ g/cm^3 is the density of the adsorbed (dry) polymer layer and l is the dry layer thickness (in cm) obtained from the ellipsometry.

The hydration of the polymer in the brush immersed in the aqueous phase was calculated from the combination of ellipsometry and QCM-D data using

$$\text{hydration} = 100 - 100\,\frac{m^{(\text{ellipsometry})}}{m^{\text{QCM-D}}} \tag{19}$$

where $m^{\text{QCM-D}}$ is the mass obtained with QCM-D.

As can be seen from the data presented in Table 1, and in accordance to the prediction of our theory, for approximately the same grafting density, $s^{(\text{dendron})} \approx s^{(\text{linear})}$, the hydrated mass of

the brush formed by linear chains is approximately twice larger than that of the brush formed by dendritic chains. Consequently, the polymer volume fraction in the dendritic brush is twice larger than that in the brush formed by linear chains. According to eq 16, the ratio of polymer volume fraction in the dendritic brush to that in the brush formed by linear chains at the same grafting density depends solely on the degree of branching, quantified by the ratio $N/\mathcal{N} \geq 1$ and should be found in the range from $(N/\mathcal{N})^{1/3}$ to $(N/\mathcal{N})^{2/3}$. For the particular architecture of the dendrons used in the current experiments we can estimate that the degree of branching $N/\mathcal{N} \approx 6$. As a result, the ratio of polymer concentrations in dendritic and linear brushes is expected to be found in the range $1.8 \leq (c^{\mathrm{dendr}}/c^{\mathrm{linear}}) \leq 3.3$, where the lower and the upper boundaries correspond to the longest path and uniform stretching scenarios, respectively. The experimentally found value is close to that predicted by theory for moderate grafting densities which is indeed the case in the experimental situation considered here.

7. Discussion and Conclusions

We have obtained a detailed picture for the structural organization of polymer brushes formed by dendritic macromolecules (dendrons) which are grafted by the terminal segments of the root spacer to a planar surface. We have combined the numberical SF-SCF approach, for which no preassumptions are needed with respect to the local stretching of the chains, with an analysis based on the much more simple boxlike model. In the latter approach, different results are found depending on the type of stretching scenario that is envisioned. Some of our findings prove that the use of a simple boxlike model with a preassumption of how the dendrons are stretched[52] may lead to erroneous results for dendritic polymer brushes. Yet the boxlike model can be used to rationalize some of the numerical SCF results.

Similar to brushes formed by end-grafted linear polymer chains, the structure of dendritic brushes is characterized by the extension of grafted macromolecule in the direction perpendicular to the surface. The macromolecules are stretched due to the crowding of the segments. The equilibrium structure of the brush is found, as usual, as a balance of the conformational entropy penalty with the free energy of excluded volume interactions in the brush.

In linear chains, the elastic tension propagates along the contour of the chain and progressively decreases from the grafting point to the free end. The local tension in the chain is a function of the ranking number of the segments ("chemical distance") counted from the grafted segment at the surface and depends on the position of the free end. A smoothly decrease in the overall polymer concentration as a function of the distance from the surface (the well-known parabolic profile) is accompanied by a wide distribution (large fluctuations) in the overall extension of individual chains in the brush. An increase in the grafting density leads to a progressive shift in the maximum in the density distribution of the free ends toward the periphery of the brush and to an increase in the average stretching of the chains in the brush. Therefore, a highly simplified boxlike model, which smears out the details of internal structural organization of the brush by preassuming the equal and uniform stretching of all the chains in the brush, gives a correct prediction for the average brush thickness as a function of the grafting density.

The distribution of the elastic tension in the brushes made of end-grafted branched macromolecules essentially depends on their topology. In particular, for hierarchically branched (dendritic, randomly, or hyperbranched) macromolecules, there are multiple end points, which implies that there are multiple elastic paths passing from the grafting point to the terminal segments. In the case of regular dendrons, considered here, all the elastic paths are terminated by the last generation spacers and thus have the same contour length. At a given maximal distance from the grafted end to one of the terminal points, different elastic paths within one macromolecule may be stretched differently.

An application of the boxlike model to the polymer brush formed by branched macromolecules implies a certain preassumption concerning the distribution of the elastic tension within end-grafted branched macromolecules. Two limiting scenarios, corresponding to the minimal and maximal conformational entropy loss, at a given overall extension of the dendron, were considered. The minimal entropy loss is characterized by the stretching of only one longest elastic path, whereas all the side paths remain nonstretched. The highest entropy loss scenario envisions equal stretching of all the elastic paths. All other possible intramolecular distributions of the elastic tension should be intermediate between these two limiting scenarios and therefore should have some intermediate conformational entropy loss.

The scaling exponent for the dependences of the average polymer concentration in brushes on the grafting density, as obtained for the two stretching scenarios, is the same as for the brushes formed by linear chains, i.e., $\langle c \rangle \sim s^{-2/3}$. However, the conformational entropy of a dendron in the brush obeys, for the two stretching scenarios, different scaling dependences on the degree of branching, $N/\mathcal{N}$. An increase in the grafting density may result in a changes in the character of how the intramolecular elastic tension is distributed. As a result, the scaling of the average concentration in the brush $\langle c \rangle$ with the grafting density $1/s$ may deviate from the value 2/3 predicted by the boxlike model. This behavior has been found in our SF-SCF calculations that point, for an increase of the grafting density, to the gradual crossover from the stretching of the longest path only to the homogeneously distributed stretching. Hence, upon an increase in grafting density, gradually more and more spacers become stretched. This trend is most pronounced for the dendrons with a high functionality of branching and/or a large number of generations.

The analysis of the experimental results concerning the relative degrees of hydration of dendritic brushes in comparison to linear PEG brushes indicates that, in the experimentally attainable (moderate) range of grafting densities, the tension is localized predominantly in the longest elastic path of the dendrons. This result is in line with our theoretical findings.

The detailed SCF analysis of the internal structural organization of the dendritic brush unambiguously indicates that at high grafting densities the packing of dendritic macromolecules in a planar brush leads to a relatively uniform, which is plateau-like, distribution of the monomer density. This implies an intrabrush segregation of dendrons having contributions that belong to different subpopulations. For the brushes formed by the first-generation dendrons we made a detailed analysis of this phenomenon. Near the surface (that is, the proximal region) the brush is enriched by segments of the first population, that is, by dendrons that have only weakly extended spacers (including the root spacer). The second population of the dendrons are characterized by a strongly, at high grafting density almost completely, stretched root spacer and are predominantly found in the periphery of the brush. In brushes formed by dendrons of higher generations, multimodal distributions were found both for the terminal segments and for the branching points. These correspond to multiple populations which are stratified throughout the brush.

Interestingly, the SCF analysis of the end-segment and branching points distributions in a free dendrimer[57] points to a wide unimodal (with one pronounced maximum) distribution of the end point throughout the volume of the dendrimer. This behavior is similar to quasi-critical fluctuations of linear chains in a planar polymer brush,[37,38,41] where the polymer density decreases

as a nonpower law function of a distance from the grafting plane. In the dendrimer, the monomer units density weakly decreases as a function of the distance from the center due to increasing number of branches in outer generations. A very different structure is found in a star polymer: In the latter case the end segments are distributed in the peripheral region of the corona while a pronounced dead zone (free of the terminal segments of the arms) is found close to the center of the star.[42,60,61] The appearance of this dead zone is explained by the power law radial decay of the polymer density. For planar brushes composed of homodisperse, linear chains, one may find a bimodal distribution of the end segments when the brush is confined, e.g., compressed by a second surface.[62] The analogy with the dendritic brush is appealing. In dendritic polymer brushes, the role of the compressive force is played by the excess polymer density at the periphery of the brush which is generated by the branching of subsequent generations.

Acknowledgment. This work has been partially supported within Scientific and Technological Cooperation Program Switzerland-Russia, project "Experimental studies and theoretical modelling of amphiphilic di/triblock and dendritic functional polymers at surfaces: influence of interfacial architecture on biological response", Grant Agreement No. 128308, and by the Russian Foundation for Basic Research (Grant 08-03-00336).

References and Notes

(1) Birshtein, T. M.; Amoskov, V. M. *Polym. Sci. U.S.S.R.* **2000**, *42*, 172–207.
(2) Halperin, A.; Tirrell, M.; Lodge, T. *Adv. Polym. Sci.* **1990**, *31*, 100.
(3) Borisov, O. V.; Zhulina, E. B. Responsive polymer brushes: a theoretical outlook. In *Smart Polymers: Production, Study and Applications in Biotechnology and Biomedicine*; Mattiasson, B., Galaev, I., Eds.; CRC Press: Boca Raton, FL, 2006.
(4) Napper, D. H. *Polymeric Stabilization of Colloidal Dispersions*; Academic Press: London, 1985.
(5) Fleer, G. J.; Cohen Stuart, M. A.; Scheutjens, J. M. H. M.; Cosgrove, T.; Vincent, B. *Polymers at Interfaces*; Chapman & Hall: London, 1993.
(6) Klein, J.; Kumacheva, E.; Mahalu, D.; Perahia, D.; Fetters, L. *Nature* **1994**, *370*, 634.
(7) Schorr, P.; Kwan, T.; Kilbey, M.; Shaqfeh, S. G.; Tirrell, M. *Macromolecules* **2003**, *36*, 389.
(8) Raviv, U.; Klein, J. *Science* **2002**, *297*, 1540.
(9) Lee, S.; Spencer, N. D. *Science* **2008**, *319*, 575.
(10) Cheng, M.; Briscoe, W. H.; Armes, S. P.; Klein, J. *Science* **2009**, *323*, 1698.
(11) Ratner, B. D.; Hoffman, A. S.; Schoen, F. J. *Biomaterial Science. An Introduction to Materials in Medicine*; Academic Press: London, 2004.
(12) Betageri, G. V.; Jenkins, S. A.; Parsons, D. L. *Lyposome Drug Delivery Systems*; CRC Press: London, 1993.
(13) *Stealth Lyposomes*; Lasic, D., Martin, F., Eds.; CRC Press: Boca Raton, FL, 1995.
(14) Cooper, J. M.; Cass, A. E. G. *Biosensors*; University Press: Oxford, 2004.
(15) Abu-Lail, N. I.; Camesano, T. A. *Biomacromolecules* **2003**, *4*, 1000.
(16) Ng, L.; Grodzinsky, A. J.; Patwari, P.; Sandy, J.; Plaas, A.; Ortiz, C. *J. Struct. Biol.* **2003**, *143*, 242.
(17) Fuchs, E.; Cleveland, D. W. *Science* **1998**, *279*, 514.
(18) Zhulina, E. B.; Leermakers, F. A. M. *Soft Matter* **2009**, *5*, 2836.
(19) Zhulina, E. B.; Leermakers, F. A. M. *Biophys. J.* **2007**, *93*, 1421.
(20) Zhulina, E. B.; Leermakers, F. A. M. *Biophys. J.* **2007**, *93*, 1452.
(21) Zhulina, E. B.; Leermakers, F. A. M. *Biophys. J.* **2010**, *98*, 462.
(22) Hamley, I. W. *The Physics of Block Copolymers*; Oxford University Press: New York, 1998.
(23) Alexander, S. *J. Phys.* (*Paris*) **1977**, *38*, 983.
(24) de Gennes, P.G . *Macromolecules* **1980**, *13*, 1069.
(25) Birshtein, T. M.; Zhulina, E. B. *Polym. Sci. U.S.S.R.* **1983**, *A25*, 2165–2174.
(26) Birshtein, T. M.; Zhulina, E. B. *Polym. Sci. U.S.S.R.* **1999**, *A41*, 2165–2174.
(27) Daoud, M.; Cotton, J. P. *J. Phys.* (*Paris*) **1982**, *43*, 531.
(28) Birshtein, T. M.; Zhulina, E. B. *Polymer* **1984**, *25*, 1453.
(29) Borisov, O. V.; Birshtein, T. M.; Zhulina, E. B. *Polym. Sci. U.S.S.R.* **1988**, *30*, 772.
(30) Pincus, P. *Macromolecules* **1991**, *24*, 2912.
(31) Borisov, O. V.; Birshtein, T. M.; Zhulina, E. B. *J. Phys. II* **1991**, *1*, 521.
(32) Ballauff, M.; Borisov, O. V. *Curr. Opin. Colloid Interface Sci.* **2006**, *11*, 316.
(33) Zhulina, E. B.; Birshtein, T. M.; Borisov, O. V. *Macromolecules* **1995**, *28*, 1491–1499.
(34) Amoskov, V. M.; Birshtein, T. M.; Pryamitsyn, V. A. *Macromolecules* **1996**, *29*, 7240.
(35) Amoskov, V. A.; Birshtein, T. M. *Polym. Sci. U.S.S.R.* **2000**, *A42*, 392–404.
(36) Wijmans, C. M.; Leermakers, F. A. M.; Fleer, G. J. *J. Chem. Phys.* **1994**, *101*, 8214–8223.
(37) Skvortsov, A. M.; Pavlushkov, I. V.; Gorbunov, A. A.; Zhulina, E. B.; Borisov, O. V.; Pryamitsyn, V. A. *Polym. Sci. U.S.S.R.* **1988**, *30*, 1706.
(38) Milner, S. T.; Witten, T. A.; Cates, M. *Macromolecules* **1988**, *21*, 2610.
(39) Zhulina, E. B.; Pryamitsyn, V. A.; Borisov, O. V. *Polym. Sci. U.S.S.R.* **1989**, *31*, 205.
(40) Zhulina, E. B.; Borisov, O. V.; Pryamitsyn, V. A.; Birshtein, T. M. *Macromolecules* **1991**, *24*, 140.
(41) Klushin, L. I.; Skvortsov, A. M. *Macromolecules* **1991**, *24*, 1549.
(42) Semenov, A. N. *Sov. Phys. JETP* **1985**, *61*, 733.
(43) Lai, P. Y.; Zhulina, E.B. . *Macromolecules* **1992**, *25*, 5201.
(44) Amoskov, V. M.; Pryamitsyn, V. A. *J. Chem. Soc., Faraday Trans.* **1994**, *90*, 889.
(45) Amoskov, V. M.; Pryamitsyn, V. A. *Polym. Sci. U.S.S.R., Ser. A* **1995**, *37*, 731.
(46) Amoskov, V. M.; Pryamitsyn, V. A. *Macromol. Theory Simul.* **2003**, *12*, 223.
(47) Biesheuvel, P. M.; de Vos, W. M.; Amoskov, V. M. *Macromolecules* **2008**, *41*, 5070.
(48) Merlitz, H.; He, G. L.; Wu, C. X.; Sommer, J.-U. *Macromolecules* **2008**, *41*, 5070.
(49) Merlitz, H.; He, G. L.; Wu, C. X.; Sommer, J.-U. *Phys. Rev. Lett.* **2009**, *102*, 115702.
(50) Wijmans, C. W. Copolymers at the solid-liquid interface. PhD Thesis, Wageningen University, 1994; Chapter 1.
(51) Zhulina, E. B.; Vilgis, T. *Macromolecules* **1995**, *28*, 1008.
(52) Kröger, M.; Peleg, O.; Halperin, A. *Macromolecules* **2010**, *43*, 6213.
(53) Ballauff, M.; Likos, C. *Angew. Chem., Int. Ed.* **2004**, *43*, 2998.
(54) de Gennes, P.-G.; Hervet, H. *J. Phys.* (*Paris*) **1983**, *44*, L351.
(55) Mansfield, M. L.; Klushin, L. I. *Macromolecules* **1993**, *26*, 4262.
(56) Boris, D.; Rubinstein, M. *Macromolecules* **1996**, *29*, 7251.
(57) Klein Wolterink, J.; van Male, J.; Daoud, M.; Borisov, O. V. *Macromolecules* **2003**, *36*, 6624.
(58) de Gennes, P. G. *Scaling Concepts in Polymer Physics*; Cornell University Press: Ithaca, NY, 1979.
(59) Birshtein, T. M.; Liatskaya, Y. V.; Zhulina, E. B. *Polymer* **1990**, *31*, 2158.
(60) Wijmans, C. M.; Zhulina, E. B. *Macromolecules* **1993**, *26*, 7214.
(61) Grest, G. A.; Kremer, K.; Milner, S. T.; Witten, T. A. *Macromolecules* **1989**, *22*, 1904.
(62) Zhulina, E. B.; Borisov, O. V.; Pryamitsyn, V. A. *J. Colloid Interface Sci.* **1990**, *137*, 495.